Nuclear Inst. and Methods in Physics Research, A 904 (2018) 179–187

Contents lists available at ScienceDirect

Nuclear Inst. and Methods in Physics Research, A

journal homepage: www.elsevier.com/locate/nima

# $H^-$ extraction systems for CERN's Linac4 $H^-$ ion source

D.A. Fink [a,*], T. Kalvas [b], J. Lettry [a], Ø. Midttun [c], D. Noll [a]

[a] CERN, BE-ABP-HSL, 1211 Geneva 23, Switzerland
[b] University of Jyväskylä, Department of Physics, 40100 Jyväskylä, Finland
[c] University of Bergen, Bergen, Norway

ARTICLE INFO

*Keywords:*
$H^-$ source
$H^-$ extraction system
LEBT
Linear accelerator
Linac4
IBSimu

ABSTRACT

Linac4 is a 160 MeV linear $H^-$ accelerator at CERN. It is an essential part of the beam luminosity upgrade of the Large Hadron Collider (LHC) and will be the primary injector into the chain of circular accelerators. It aims at increasing the beam brightness by a factor of 2, when compared to the currently used 50 MeV linear proton accelerator, Linac2.

Linac4's ion source is a cesiated RF-plasma $H^-$ ion source. Several beam extraction systems were designed for $H^-$ beams of 45 keV energy, 50 mA intensity and an electron to $H^-$ ratio smaller than 5. The goal was to extract a beam with an rms-emittance of $0.25\pi$ mm mrad.

One of the main challenges in designing an $H^-$ extraction system is dumping of the co-extracted electrons. Separating the electrons from the negative ions as early as possible reduces space-charge induced emittance-growth. However, a strong magnetic field close to the extraction might cause unnecessary strong deflection in a region of low beam energy. For this purpose a novel magnetic configuration was designed using a magnetic shield between the magnetic fields of the source and the electron dump, which conserves the filter field strength to keep the electron to $H^-$ ratio low and effectively dumps the co-extracted electrons. Magnetic configuration and beam trajectories were calculated using the TOSCA Opera 3D code and IBSimu, respectively. Three extraction systems will be discussed in terms of electron dumping efficiency, emittance and transport through the extraction system and LEBT to the RFQ and compared to the simulations.

An improved emittance conservation through the extraction system and LEBT is predicted and further design improvements are proposed. Measurements show that the novel electron dump successfully traps the co-extracted electrons.

## 1. Introduction

The extraction system of an ion source is the first stage of a particle accelerator. It is thus responsible for early beam formation and defines the initial intensity and beam quality that is passed down the chain of accelerating structures. The challenge presented in this paper is to design a high current, low emittance $H^-$ beam extraction system that will be used at Linac4.

Linac4 is a normal conducting linear $H^-$ accelerator that will replace the existing linear proton accelerator, Linac2, to become the main injector for CERN's accelerator complex [1]. Increasing the injection energy into the first circular accelerator, the Proton Synchrotron Booster (PSB), from Linac2's 50 MeV to Linac4's 160 MeV allows doubling the beam brightness inside the PSB. The increased beam brightness will eventually translate into an increased beam luminosity inside the LHC [2].

Using $H^-$ to inject protons into the PSB via charge-exchange injection is advantageous for two reasons: first, it allows for accumulating more protons in the same phase space without significantly increasing the emittance and thus increasing the luminosity of the LHC experiment and second, it reduces safety concerns due to the lower beam losses caused by the stripping process when compared to direct proton injection.

The Linac4 ion source is a cesiated molybdenum-surface radio-frequency-plasma $H^-$ ion source. It produces $H^-$ through the volume and surface production mechanisms [3–5]. An $H^-$ production of 50 mA and more has been demonstrated with this setup [6].

The development of an $H^-$ ion source that meets Linac4's requirements is challenging: 400 μs beam pulses at 0.8 Hz with intensities of up to 40 mA $H^-$ [7]. The beam extracted from the source should have a normalized rms-emittance of less than $0.25\,\pi$ mm mrad and must be matched to the acceptance of the Radio-Frequency Quadrupole (RFQ) of $2.6\,\pi$ mm mrad. At the same time the injector should have an availability of 99% over the LHC's run period [8].

Compared to extraction systems for positive ions, the design for $H^-$ ions is more complicated: the co-extracted electrons need to be

* Current address: A.D.A.M. SA, Meyrin, Switzerland.
*E-mail address:* daniel.fink@cern.ch (D.A. Fink).

https://doi.org/10.1016/j.nima.2018.07.046
Received 13 June 2018; Received in revised form 15 July 2018; Accepted 17 July 2018
Available online 21 July 2018

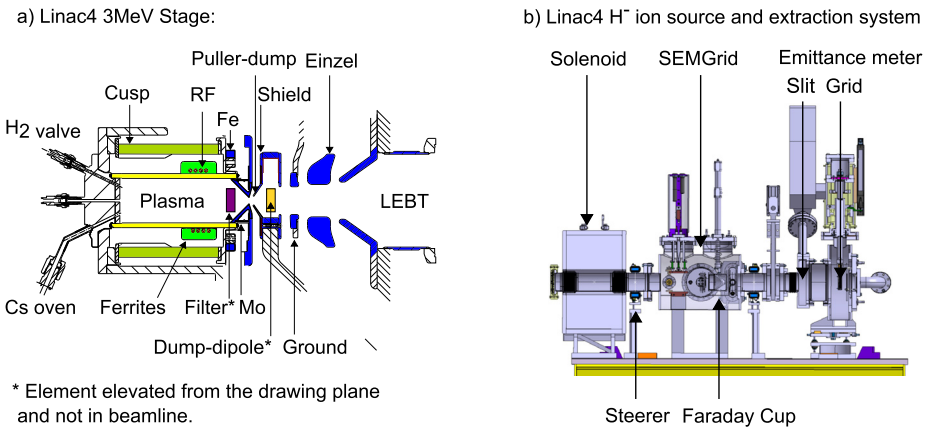


**Fig. 1.** (a) Top view of the Linac4 $H^-$ ion source and the extraction system IS03b. (b) Linac4 test stand with a single solenoid LEBT and beam diagnostics. For the measurements with IS03b, the diagnostic tank was removed and the slit and grid emittance meter was moved closer to the solenoid.

separated from the $H^-$ beam and dumped. This requires additional magnetic dipole fields in the vicinity of the extraction region, which are superimposed with the magnetic fields of the source. Inside the plasma chamber, there is a multicusp field for confinement and a dipole filter field [3,9] for suppressing the high energy electrons in the vicinity of the extraction aperture and therefore reducing the destruction of the fragile $H^-$ ions. The filter field is optimized to produce a high $H^-$ current while maintaining a low electron to $H^-$ ion ratio (e/$H^-$ ratio). The magnetic field in the beam extraction system should be formed to deflect and dump the electrons while only minimally affecting the $H^-$ trajectories. Electrons are considered to be dumped safely when no secondary electrons escape the dump and the deposited power density of the electron beam is below the damage threshold for sublimation of the dump material.

A previous revision of the extraction system for the Linac4 $H^-$ ion source was presented in Ref. [10], which features a decelerating *einzel-lens electron dump*. In this paper, we compare three new revisions: IS02, IS03a and IS03b. The beam trajectories are simulated and provide electron dumping and $H^-$ transport efficiencies and the $H^-$ beam emittance. The simulation results are used to interpret experimental results which are also presented. Possible improvements to the existing setups are discussed at the end of this article.

## 2. Simulation tools

The most important aspect in simulating the extraction of negative hydrogen ions from a plasma is an accurate prediction of the shape of the plasma-beam boundary, the plasma meniscus. Recently, the beam formation region has been simulated with 3D particle-in-cell (PIC) Monte Carlo codes, ONYX and KEIO-BFX, but CPU times of several days to weeks are inconvenient for a systematic optimization of the geometries [11,12]. A more suitable tool for such a task is the Ion Beam Simulator (IBSimu) [13]. This code does not take into account all the physical processes affecting the plasma meniscus, but provides a sufficient approximation of the plasma meniscus for design purposes. The code self-consistently calculates the plasma meniscus for positive and negative particle extraction and tracks charged particles. It solves the Poisson equation with the beam space charge coupled with an analytic formulation for the compensating charge density in the plasma using the Finite Difference Method (FDM). Input parameters for the plasma calculations are plasma potential ($\Phi_P = 7.5\,V$), initial energy of tracked particles at the sheath edge ($E = 5\,eV$), ion temperature ($T_t = 0.5\,eV$), the temperature of the thermal positive ions ($T_+ = 1\,eV$) and the fraction of the compensating particles ($R_f = 0.5$). A detailed discussion of the input parameters can be found in Ref. [14]. Surface ionization mechanisms are not implemented into the model. These plasma parameters were benchmarked against experiments for the previous Linac4 extraction system, IS01, [10] and were not changed for the simulations presented in this article.

IBSimu uses a square and uniform 3D-mesh. In order to save computing time, the simulations were split up in different sections with increasing mesh size according to the required precision: 0.25 mm or 0.5 mm in the vicinity of the plasma aperture, 0.5 mm for the extraction system, and 1 mm for the transport through the Low Energy Beam Transport (LEBT). The trajectory density was kept at a minimum of 100 trajectories per mesh volume cell. For the calculation of the space-charge compensation by residual gas inside the LEBT, a Monte-Carlo routine was implemented. A detailed description of this procedure can be found in Ref. [15].

Magnetic fields were calculated by the commercial finite-element mesh simulation code Opera-3d TOSCA from Vector fields [16] and field maps were imported into IBSimu for particle tracking.

## 3. Setup

Fig. 1(a) shows the cesiated radio-frequency-plasma $H^-$ ion source together with the extraction system IS03b. Hydrogen is injected into the $Al_2O_3$ plasma chamber using a pulsed piezo valve. A 4 to 5 turn RF-solenoid antenna operating with a frequency of $2 \pm 0.1$ MHz and a power of typically 30 kW to 50 kW ignites and heats the hydrogen plasma. A magnetic cusp-field created by permanent magnets in a Halbach-configuration confines the plasma [17]. Viewing ports are available for studying the plasma parameters using optical emission spectroscopy [18–20]. A dipole filter field created by permanent magnets prevents fast electrons from reaching the extraction zone [9]. The molybdenum surface surrounding the plasma aperture is cesiated by injecting cesium (Cs) into the plasma chamber by a cesium oven. Its low work function acts as a source of $H^-$ ions via surface ionization and reduces co-extracted electrons.

The extraction systems discussed in this paper are composed of the following elements: a combined extraction and dumping electrode (*puller-dump*), a ground electrode, an accelerating einzel lens and a ground electrode at the entrance of the LEBT.

The LEBT consists of two focusing solenoid magnets for matching of the beam into the subsequent RFQ and contains the following beam diagnostic devices: a Faraday cup (FC), a Secondary electron Emission Monitor Grid (SEMGrid) for beam profile measurements, and a Beam Current Transformer (BCT) for beam intensity measurements at the entrance of the RFQ.

The Linac4 ion source test stand allows for development work and beam dynamic studies without interfering with the Linac4 operation [21]. Fig. 1(b) shows a cutaway of the LEBT of the test stand. The LEBT of the test stand is equipped with one solenoid for focusing, while the second solenoid of the Linac4 frontend is replaced with a slit and

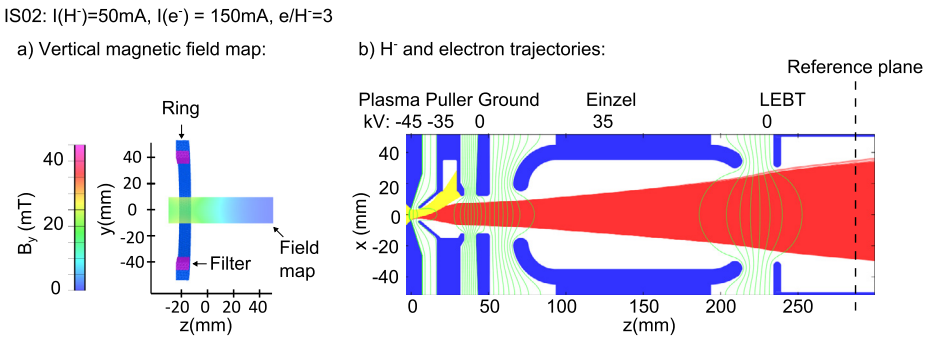


**Fig. 2.** IS02 extraction system. (a) Field map of the vertical magnetic field component in the vertical plane. The relevant magnetic elements are labeled. The strength of the magnetic field is indicated by the field map. (b) $H^-$ (red) and electron (yellow) trajectories in the horizontal plane. Blue elements are electrodes and electrostatic equipotentials are drawn with green lines. Note the limited deflection: electrons do not properly enter into the electron dump. (For interpretation of the references to color in this figure legend, the reader is referred to the web version of this article.)

grid emittance meter [22]. For the measurements with IS03b presented in this paper, the slit and grid emittance meter was installed right after the solenoid.

## 4. Extraction systems

Extraction systems for $H^-$ ion sources need to provide the beam intensities and optical properties required by the accelerator and efficiently separate and dump the co-extracted electrons. These requirements lead to conflicting design choices: the magnetic dipole field needed for electron dumping may compromise the efficiency of the filter field and add an angle and an offset to the beam. In addition, the required space for the electron dump is a constraint for the design of the ion optical elements needed to shape the beam in order to optimize the transport through the LEBT. Thus, the electron dump and the ion optics need to be carefully optimized as an entity to satisfy both requirements.

The first extraction system operated at Linac4, IS01, was designed for a volume production $H^-$-source with beam intensities of 20–30 mA $H^-$ and high electron to $H^-$ ratios of 20–60 [10]. In this design, the co-extracted electrons were steered into a magnetic einzel-lens dump to remove the electrons from the beam and focusing the $H^-$ beam. IS01 was successfully and reliably operated during the commissioning of Linac4. But it became conclusive that for higher beam intensities and larger beam sizes, the emittance-growth inside the einzel lens due to space-charge and aberration will be too strong. Simulations with IBSimu predicted that for a beam with 50 mA $H^-$ intensity and an e/$H^-$ ratio of 3, the expected emittance is $0.8\,\pi$ mm mrad at the entrance of the solenoid. This exceeds the design criteria and it was decided to upgrade the extraction system to match higher beam intensities and lower e/$H^-$ ratios expected from a cesiated RF-plasma $H^-$ source.

The extraction systems discussed in here are *puller-dump* type extraction systems, which dump the electrons into a dedicated slot in the extraction electrode. The early separation of co-extracted electrons and avoidance of a decelerating einzel lens improves the emittance-preservation due to the reduced space-charge contribution of the electrons and due to reduced aberration, respectively. The major differences between the extraction systems are the different magnetic fields, the dump designs and the length of the extraction systems. IS02 uses only the filter-field for dumping of the co-extracted electrodes. IS03a is of shorter length and has additional dipole magnets for electron dumping and a magnetic shield separating the filter and dumping fields for dumping of the electrons. IS03b is further optimized by improving the dump design and the ion optics for transport to the LEBT.

The beam simulations were performed using a reference beam with 50 mA $H^-$ intensity and an e/$H^-$ ratio of 3.

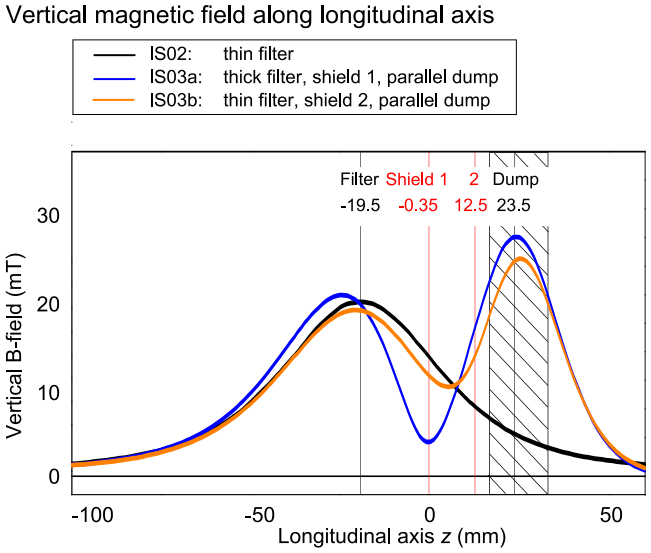


**Fig. 3.** The vertical magnetic field strength as a function of location on the $z$-axis for different magnetic configurations. Positions of the magnets (filter and dump) and the magnetic shields (IS03a:1 and IS03b:2) are given. The shaded area indicates the position and the length of the IS03b dump.

### 4.1. IS02 extraction system

The overall length of IS02, measuring from the plasma electrode to the LEBT aperture, is 234 mm. The plasma electrode is operated at −45 kV and has an aperture diameter of 6.5 mm. The electrode is beveled with an angle of 15° to minimize the non-linear focusing of the electric field in the extraction gap causing emittance growth. The tip of the extraction electrode is 4.5 mm away from the plasma electrode. Nominally, the extraction electrode is operated at −35 kV with a 10 kV potential difference to the source, leading to a slightly concave plasma-beam boundary (meniscus) that weakly focuses the extracted $H^-$ and electrons.

Fig. 2(a) shows the calculated magnetic field map from the filter field up to the electron dump and Fig. 2(b) shows the calculated trajectories of the $H^-$ ions and electrons of the reference beam. Electrons are separated from the $H^-$ ions by the filter field that is protruding into the extraction region. The filter field is generated by two permanent dipole magnets (NdFeB, length (in $x$) $l = 56$ mm, thickness (in $y$) $t = 5.8$ mm, width (in $z$) $w = 10$ mm) that are mounted within the source 20 mm from the plasma aperture in the vertical plane around the plasma chamber with each magnet $d = 40.2$ mm from the beam axis. The return flux is guided by a soft iron ring. As shown in Fig. 3 the field along the $z$-axis is

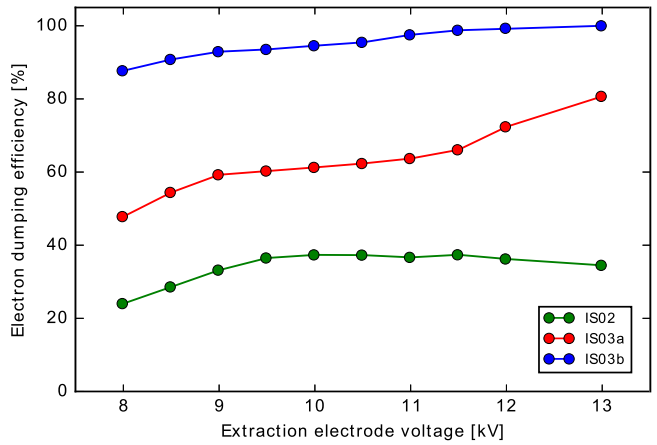


**Fig. 4.** Comparison of the dumping efficiencies of the co-extracted electrons for the extraction systems IS02, IS03a and IS03b.

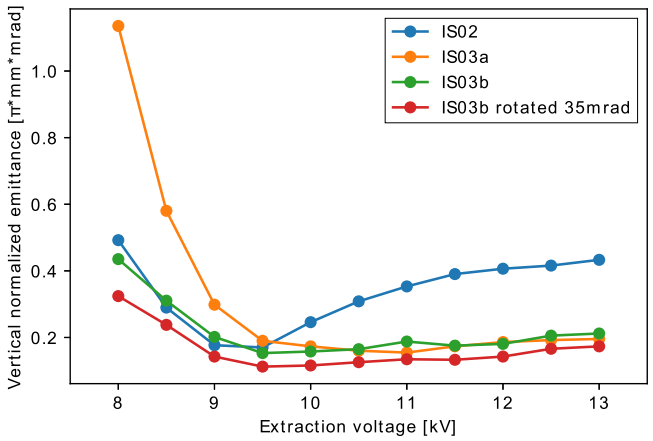


**Fig. 5.** Simulated normalized emittances as a function of the extraction voltage. The values were taken in the vertical plane 50 mm downstream of the LEBT entrance for extraction system IS02, IS03a, IS03b and IS03b with rotated plasma- and puller electrode.

symmetric and peaks at the position of the filter magnets. At the plasma aperture ($z = 0$) the field-strength is 13 mT.

The extraction electrode has a slot with dimensions $l \times h \times w = 11 \times 23 \times 35$ mm$^3$ for dumping the electrons. The electron dumping efficiencies of the *puller-dump* designs are compared in Fig. 4. For IS02, the 20–40% dumping efficiency is defined as the fraction of electrons safely dumped in the slot. The electrons missing the slot are either backscattered or generate secondary electrons that may be post accelerated. After the dump, a ground electrode accelerates the $H^-$ ions to 45 keV energy. The long accelerating einzel lens is designed to be operated with up to 35 kV to transport the ions into the LEBT.

Fig. 5 shows the emittances as a function of the extraction voltage in the vertical plane 50 mm downstream of the LEBT entrance for the reference beam ($H^-$ intensity 50 mA, e/$H^-$ ratio of 3). For these simulations, the current of the LEBT solenoid was set to 0 A for a better comparison of the extraction systems, but it should be noted that the transverse emittance will increase in the presence of a solenoid field for two reasons: first, the field strength of the solenoid increases with distance to the beam axis. Thus, for large beams, the outer particles will experience a stronger focusing than the particles near the beam center. Second, the non-homogeneous electrostatic field of the einzel lens overlaps with the start of the solenoid field leading to non-linear effects and coupling between the longitudinal beam energy and transverse emittance. The IS02 rms-emittance has a minimum value of $0.2\,\pi$ mm mrad using an extraction voltage of −9.5 kV. With lower extraction voltages, the emittance is larger due to a too weak extraction field, which leads to highly diverging beams and aberrations between the *puller-dump* and the ground electrode. If the extraction potential is higher, the plasma sheath becomes concave, which causes non-linear focusing and increased emittance already at beam formation. Compared to the simulations for IS01, this is an improvement in emittance of a factor of 4.

#### 4.1.1. IS02 performance

IS02 was operated at Linac4 from June 2014 to June 2015. A copy of IS02 was operated at the Linac4 test stand from October 2014 to March 2015. The performance at the test stand was promising. After cesiation the intensities of the ion beam reached 45 mA $H^-$ with an e/$H^-$ ratio of 1 to 2.

Throughout the operation of IS02 a high current was measured at the power supply of the einzel lens. This is due to the low efficiency of the electron dumping process as predicted by the simulations shown in Fig. 4. These electrons that do not enter the intended slot of the electron dump are either directly back-scattered or produce secondary electrons, which are then accelerated towards the einzel lens. When the einzel lens was operated at its nominal voltage of 35 kV frequent high voltage breakdowns were observed, making an einzel lens voltage reduction necessary.

Fig. 6 shows measurements and simulations of the phase space of a 46 mA $H^-$ beam with an e/$H^-$ ratio of 1. The measurements were taken with the slit and grid emittance meter at the Linac4 ion source test stand. $H_2$ was injected into the LEBT for reaching $1 \cdot 10^{-6}$ mbar pressure, improving the space charge compensation [15]. The extraction voltage and the einzel lens were kept at 9.5 kV and 32.2 kV, respectively. Fig. 6(a) shows the simulated trajectories up to the slit of the emittance meter for a solenoid current of 97 A. A mesh size of 0.5 mm was used up to the einzel lens to guarantee accuracy of the simulated meniscus and electric field in the proximity of the electrodes. After this, a mesh size of 1 mm was used. The simulations predict that the solenoid with 97 A is strong enough to focus the beam but the focusing takes place too late and the beam is scraping the beam pipe, reducing the transmission efficiency through the LEBT and possibly generating secondary electrons.

IS02 emittances for solenoid currents from 84 A to 96 A in steps of 3 A are shown in Fig. 6(b). Measurements and corresponding simulations show a good agreement in terms of phase-space area and orientation, which demonstrates the good predictive power of the simulations. A shift of 1 A in solenoid current is observed between the measurements and simulations. The simulated rms-emittances of a 46 mA beam are $0.4\pi$ mm mrad with the exception of 97 A, for which the rms emittance is $0.44\pi$ mm mrad. The measured emittances increase with solenoid currents and are between $0.59\pi$ mm mrad and $0.67\pi$ mm mrad. The systematic difference in emittance of about 50% may be due to inaccuracy of the assumptions made by IBSimu, especially the inhomogeneity of the particle flux emanating from the plasma due to the surface and volume production processes. An additional contribution may stem from the larger halo of the measured beam, but a discussion of the fractional emittances is omitted.

Both, the simulated and the measured emittances are larger than the emittances simulated without solenoid field (Fig. 5). This indicates that the solenoid field leads to a significant increase of the emittance as discussed above.

At Linac4, the typical output intensity from the source was about 40 mA with an e/$H^-$ ratio of 4 to 8. The reduced performance compared to the test stand was probably due to different cesiation conditions. The $H^-$ yield and the e/$H^-$ ratio are very sensitive to the properties of the surfaces to which the cesium layers are deposited. Of the 40 mA $H^-$ typically 30 mA were transported through the RFQ. The losses are in agreement with the emittance of about 0.6 mm mrad that was measured at the test stand.

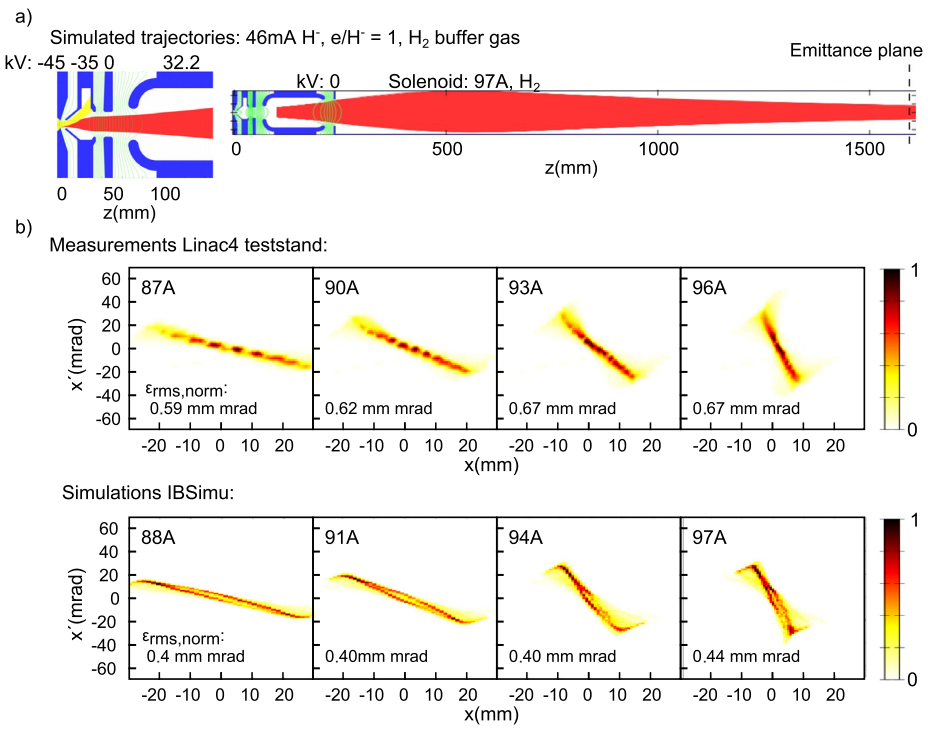


**Fig. 6.** (a) $H^-$ ions and electrons tracked through the IS02 extraction system and the LEBT. The beam intensity is 46 mA $H^-$ and the e/$H^-$ ratio is 1. The solenoid current was 96 A and the LEBT was filled with a hydrogen as buffer gas. (b) Measured and simulated IS02 phase space density for different solenoid settings. The density plot is normalized to the highest intensity. The data was taken with the slit and grid emittance meter at the Linac4 test stand.

### 4.2. IS03a extraction system

IS03a was the first iteration of a shortened extraction system, for which the distance between the plasma aperture and the LEBT entrance was reduced by 101.5 mm. It aimed at improving the dumping efficiency and the transport efficiency compared to IS02. The dump geometry is similar to that of IS02, but the einzel lens is shorter [23].

In order to improve the dumping efficiency, the extraction region was shielded from the magnetic filter field of the plasma chamber by a magnetic shield made of soft iron at the plasma aperture position. This allowed a better control over the electron dumping by adding two permanent magnets to the dump. The permanent magnets were installed 23.5 mm downstream of the plasma electrode aperture and the magnetic field is vertically oriented. The thickness of the filter field magnets was increased to 8 mm to compensate for the reduction of the filter peak field due to the soft iron shield. The effective separation of the filter- and electron-dump fields is visible in the field map of Fig. 7(a) and in Fig. 3. The emittance was expected to be below the acceptance criteria of 0.25 $\pi$ mm mrad for extraction voltages higher than 9.5 kV as shown in Fig. 5.

#### 4.2.1. IS03a performance

IS03a produced up to 50 mA $H^-$ during the Linac4 commissioning phase. Transmission of a 35 mA $H^-$ beam through the RFQ was of the order of 85% when the current was measured on the BCTs before and after the RFQ. The electron beam measured downstream of the dump was greatly reduced as expected from the improved design of the magnetic field. This is supported by the simulated dumping efficiency of 50–80% (see Fig. 4).

In contrast, the ratio of co-extracted electrons and $H^-$ ions was significantly increased compared to IS02. e/$H^-$ ratios of 2 to 13 were measured. The increased electron extraction is believed to be due to the reduced efficiency of the filter field. As shown in Fig. 7(a) and Fig. 3, the IS03a magnetic field in the proximity of the plasma aperture is 3 times lower than in the case of IS02 with a remaining magnetic field strength of only 3 mT.

### 4.3. IS03b extraction system

Ion extraction, electron dumping and transport to the LEBT was re-designed for IS03b in order to improve the electron dumping efficiency and the matching to the RFQ. Fig. 7(b) and (c) show the magnetic field map and the geometry and trajectories of the reference beam, respectively.

The goal was to improve the electron dumping efficiency and to increase the filter field strength at the plasma aperture to a magnetic field strength that is similar to that of IS02. Increasing the filter field was expected to provide higher $H^-$ production rates and lower e/$H^-$ ratios. For this purpose, the magnetic shield was moved from the plasma to the *puller-dump* electrode. Fig. 1(a) and Fig. 7(b) show the geometry and the magnetic elements present in the IS03b source and extraction system. Dumping field and filter field remain decoupled as in the case of IS03a, but the filter field extends rather undisturbed into the extraction system before the magnetic field lines are guided into the soft iron shield at the dump position. The electrons are only slightly deflected by the filter field, while the dumping is mainly achieved by the dipole of the *puller-dump* behind the magnetic shield. The positions of the filter field, shield and dumping magnets that were optimized for effective dumping are $z = -19.5$ mm, 12.5 mm, and 23.5 mm, respectively, as shown in Fig. 3. To improve the dumping efficiency, the dump slot size was increased to $l \times h \times w = 16 \times 45 \times 33$ mm$^3$. In addition, the distance from the plasma electrode to the puller electrode was decreased and the plasma electrode thickness was reduced.

The comparison of the vertical magnetic field component along the longitudinal axis shown in Fig. 3 shows that the filter field along the longitudinal axis of IS03b is similar to that of IS02.

According to the simulations of the reference beam with 50 mA $H^-$ and an e/$H^-$ ratio of 3, the dumping efficiency is 85–100% depending on the extraction voltage (see Fig. 4). The larger size of the dump leaves

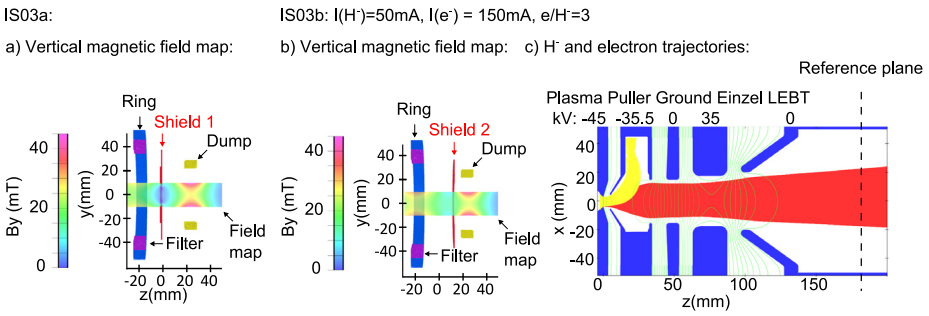


**Fig. 7.** Field maps of the vertical magnetic field component in the vertical plane for (a) IS03a and (b) IS03b. The relevant magnetic elements are labeled. The strength of the magnetic field is indicated by the field map. (c) $H^-$ and electron trajectories in the horizontal plane tracked through IS03b.

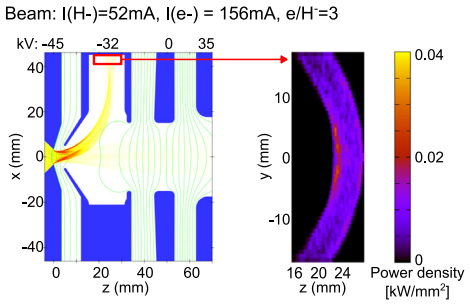


**Fig. 8.** Left: trajectory density of a simulated beam that is extracted from IS03b with an extraction voltage of 13 kV. Right: projected power density on the surface inside the dump as indicated by the red square in the left figure.

a margin for varying $H^-$ intensities and $e/H^-$ ratios, while still providing high dumping efficiencies. This is particularly important to allow for a systematic scanning of the extraction voltage in order to optimize the matching of the extraction field to the plasma.

The exit aperture of the *puller-dump* was enlarged to increase the distance of the $H^-$ beam from the electrode. This reduces aberration induced emittance-growth that can be caused by high field gradients present close to the edges of the electrodes. A careful tuning of the extraction voltage is required to obtain the optimum beam size inside the puller dump.

The einzel lens was redesigned for higher focusing strength to reduce the beam size in the LEBT: the gap length between the electrodes was shortened and the diameter was reduced. In addition, the LEBT ground electrode was moved closer to the ion source. This reduces the overlap of the strong electrostatic field of the einzel lens with the solenoid field of the LEBT, which can lead to additional emittance growth.

According to the simulations shown in Fig. 5, the emittance is within the design criteria of $0.25\,\pi$ mm mrad for extraction voltages higher than 9 kV. Larger emittances at lower extraction voltages are caused by asymmetric aberration, when the beam becomes too large inside the puller dump. High dumping efficiencies of 90–100% are achieved with extraction voltages higher than 11 kV. An increased extraction voltage translates directly into a higher beam energy and a higher power deposition onto the surfaces inside the electron dump. Therefore, the deposited power was calculated for the highest simulated extraction voltage of 13 kV (see Fig. 8). The calculated maximum power density on the dump surfaces is 0.04 kW/mm$^2$ for a 150 mA electron current. This is ten times lower than the maximum allowed power density for titanium of 0.4 kW/mm$^2$ that was calculated by dynamic thermal studies with ANSYS [10] and leaves a safety margin for operation with higher $e/H^-$ ratios and higher extraction voltages.

#### 4.3.1. IS03b performance

IS03b typically provides 50 mA $H^-$ and an electron to $H^-$ ratio between 1 and 5 depending on the level of cesiation. The $e/H^-$-ratio is significantly lower than in the case of IS03a, which can be explained by the stronger filter field in the vicinity of the extraction aperture that was preserved by the improved magnetic field design of the *puller-dump* electrode.

As predicted by the simulations shown in Fig. 4, the dumping efficiency was 100% for the extraction voltages of 9–11 kV, typically used during the operation. No secondary electrons are observed downstream of the *puller-dump*.

The emittance was measured at the Linac4 test stand as a function of the solenoid current. The trajectories for a solenoid setting of 103 A and the set of measurements are shown in Fig. 9(a) and (b), respectively. In contrast to the measurements of IS02b presented in Fig. 6, the emittance meter was brought closer to the extraction system by swapping the emittance meter with the diagnostic tank consisting of the SEMGrid and the Faraday cup. The maximum einzel lens voltage was limited to 30 kV, since higher einzel lens voltages tended to cause HV-breakdowns.

As observed for IS02, the offset of the solenoid current of $\sim 1$ A is also present in the measurements of IS03b, but the orientation of the beam in the phase space is reproduced well. The simulated beams are somewhat broader than the measured beams and the center of the beam is slightly off-axis in the negative direction.

The phase space area of the measured beams show a larger beam halo that is not reproduced by the simulations. This is reflected in a systematically higher normalized rms-emittance of typically 0.6–0.7$\pi$ mm mrad compared to the simulated emittances of about 0.35–0.4$\pi$ mm mrad. The fraction of the beam that is contained inside the halo was determined to be about 20%. After thresholding the data and the simulations to 80%, the rms-emittances become comparable. The stronger halo suggests that the measured beam gets closer to the electrodes than predicted by the simulations. This causes stronger focusing on parts of the beam by nonlinear forces. It is expected that the halo will be collimated by the RFQ.

For an extracted $H^-$ current of 41 mA, an extraction voltage of 10–11 kV, an einzel lens voltage of 30 kV and currents applied to solenoid 1 and 2 of typically 92–100 A and 110–129 A, respectively, the measured $H^-$ current at the exit of the RFQ was between 25–30 mA, which is in agreement with the emittance values exceeding the acceptance. The wide range of solenoid currents is caused by the sensitivity to the space-charge compensation level.

The rms-emittances are comparable to IS02, but it should be noted that the intensity and the solenoid currents were higher during the measurements with IS03b. Both parameters may cause additional emittance increase. In addition, the einzel lens was operated below nominal value, which leads to a larger beam size inside the solenoid and causes additional aberration in the fringe fields of the solenoid.

### 4.4. Matching of the beam to the RFQ acceptance

The $H^-$ beam properties at the RFQ matching plane result from the plasma meniscus formation, the extraction and electron dumping system and the LEBT. Therefore, for a comprehensive estimate of the efficiency

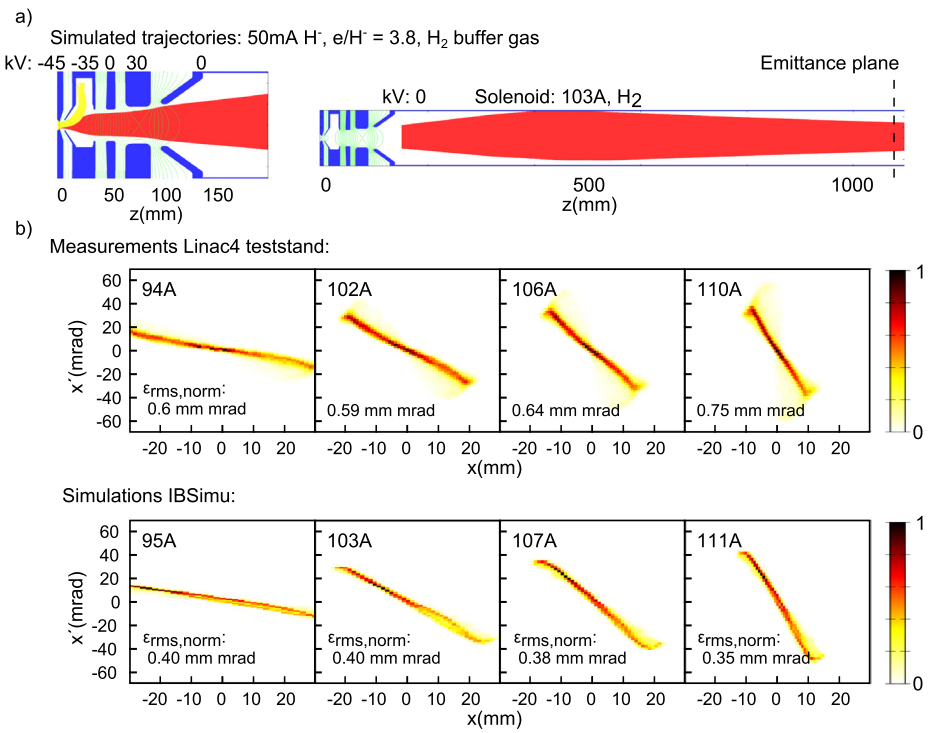


**Fig. 9.** (a) $H^-$ ions and electrons tracked through the IS03b extraction system and the LEBT. The beam intensity is 50 mA $H^-$ and the $e/H^-$ ratio is 3.8. The einzel lens was limited to 30 kV and the solenoid current was 103 A. The LEBT was filled with a hydrogen gas escaping from the source. (b) Measured and simulated IS03b phase space densities for different solenoid settings. The density plot is normalized to the highest intensity. The data was taken with the slit and grid emittance meter at the Linac4 test stand.

of the beam matching to the RFQ it is necessary to track the beam up to the matching plane.

The matching plane of the Linac4 RFQ is located 2.191 m downstream of the plasma aperture and the acceptance is defined as a phase-space ellipse with a normalized emittance of $2.6\,\pi$ mm mrad and twiss parameters $\alpha = 0.8864$ and $\beta = 2.355 \cdot 10^{-2}$ mm/mrad.

To estimate the transport efficiency, the reference beam of 50 mA $H^-$ with an $e/H^-$ ratio of 3 was tracked through the extraction system IS03b and the LEBT up to the RFQ matching plane. Puller, einzel lens voltages and both solenoid currents were optimized for highest transmission through the LEBT and matching to the RFQ. A constant $H_2$ pressure of $4 \cdot 10^{-6}$ mbar was assumed.

Fig. 10(a) shows the resulting trajectories for the IS03b extraction and LEBT parameters that led to the highest intensity inside the RFQ acceptance: puller voltage (extraction voltage) and einzel lens voltage were −34 kV (11 kV) and 35 kV, respectively and solenoid currents 1 and 2 are 95 A and 117 A, respectively. Solenoid current 1 is not high enough to prevent the outer wings of the beam from being scraped at the LEBT wall. However, the portion of the beam that is matched to the RFQ acceptance is larger than in the case of higher solenoid currents. Stronger solenoid fields cause aberration and lead to a mismatch of the beam with a larger fraction outside the RFQ acceptance. An asymmetry of the beam in the vertical plane is observed, which results from the magnetic electron dump field. At Linac4, it is possible to correct for this offset by steering magnets, but this was not taken into account in these calculations. The resulting phase-space distribution at the position of the matching plane is shown in Fig. 10. The beam is well-matched and the calculated intensity inside the RFQ acceptance is 44 mA. 6 mA of the beam is lost at the LEBT walls due to insufficient focusing.

The calculated intensity inside the RFQ acceptance is higher than the 30 mA that was experimentally observed at the end of the RFQ, which can be partly accounted on the difference on the einzel lens voltage: In the experiments the einzel lens voltage was limited to 30 kV, which leads to more divergent beams and higher losses at the LEBT walls. Additionally, the measured emittance shows a larger halo than the simulated emittance, which explains a lower fraction of $H^-$ ions inside the RFQ acceptance. Additional losses are expected to arise from the deflection by the magnetic field of the *puller-dump*, which appeared to be slightly stronger than the simulation: the asymmetric aberration inside the *puller-dump* leads to emittance growth and a larger part of the beam wing is lost at the LEBT walls.

#### 4.4.1. Improving the RFQ matching

It is possible to further improve the matching of the beam to the RFQ acceptance. Tracking the IS03b beam up to the RFQ matching plane indicates that reducing the beam size inside the LEBT and removing the deflection caused by the dump field are the most efficient means to reduce emittance growth and to improve the transmission efficiency.

Several different modifications to the IS03b einzel lens were investigated: a decelerating einzel lens with negative voltage showed the strongest focusing effect, but led to an unacceptable high emittance growth. It would be beneficial to increase the voltage of the accelerating einzel lens to values higher than 35 kV or to increase the field strength by reducing the diameter of the einzel lens. Unfortunately the einzel lens does not seem to be able to withstand the high fields in these conditions.

The deflection angle and offset due to the electron dump field can be compensated by rotating the plasma lens and *puller-dump*. According to our simulations, the rotation required for a compensation of the deflection angle is between −30 mrad and −40 mrad. The simulations shown in Fig. 5 suggest that a rotation of the plasma electrode and *puller-dump* by −35 mrad around the $y$-axis at $x = 0, z = 45$ mm caused less emittance growth than the unrotated system, which can be explained by the reduced asymmetric aberration inside the *puller-dump*.

Fig. 10b shows $H^-$ and electron trajectories of the reference beam ($H^-$ 50 mA, $e/H^-$ of 3) through the LEBT for a *puller-dump* potential of −34 kV (11 kV extraction voltage) and a rotation angle of −35 mrad. The beam inside the LEBT is more parallel in the case of the rotated IS03b extraction system, when compared to the standard IS03b. In addition to the reduced aberration inside the *puller-dump*, this leads to reduced emittance growth in the solenoid fields and reduced beam losses at the

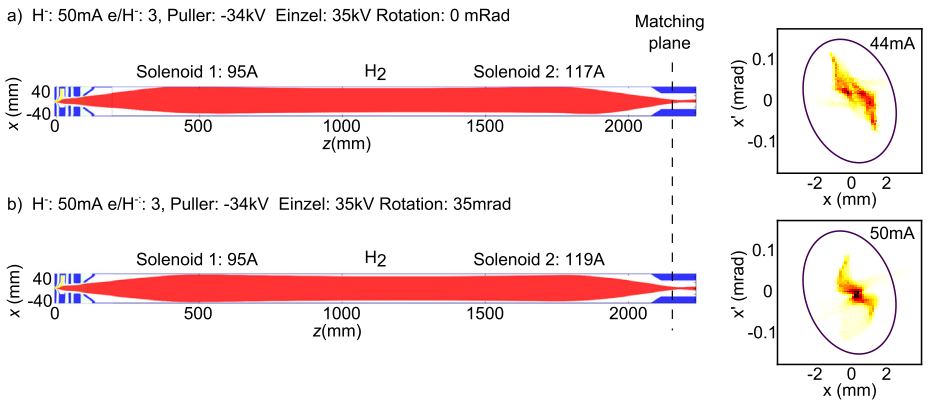


**Fig. 10.** Simulated $H^-$and electron trajectories (left) and phase-space distribution (right) at the RFQ matching plane: (a) IS03b and (b) IS03b with plasma- and *puller-dump* electrode rotated by −35 mrad.

LEBT walls. Apart from a minor portion of the beam that is lost at the wall, the transmission and matching is close to 100%. The results of these simulations suggest that a significantly improved transmission efficiency through the RFQ can be achieved by compensating for the deflection angle and offset caused by the magnetic field of the electron dump.

To further reduce the aberration inside the LEBT, the performance of the einzel lens should be improved to reduce the beam size inside the LEBT. This is particularly the case if higher intensities are transported through the system. This can be achieved by a smaller einzel lens diameter or with higher einzel lens voltages. Alternatively, the einzel lens system could be removed to move the solenoids directly to the end of the *puller-dump* and closer to the source. This has the advantage that the beam size growth from the dump to the first solenoid would be greatly reduced. Additionally, the diameter of the LEBT tubes could be increased to avoid the scraping of the beam at the LEBT walls.

The halo observed in the measurements indicates that the beam is larger than predicted by the simulations. This is possibly a result of a larger beam divergence from the plasma than what is shown by the simulations. This could be mitigated by the use of higher extraction voltage or reduction in the distance of the puller to plasma electrode to decrease the beam size in the extraction assuming the halo is generated due to non-linear focusing forces. It might also be that the halo is already generated by non-uniform plasma emission and/or the non-linear forces or other effects in the proximity of the plasma sheath such as surface ionization. Surface ionized $H^-$ ions might have a higher probability of being extracted close to the edge of the plasma electrode aperture. In this case they would populate the beam halo to a larger extent than the core of the beam, thus leading to a larger emittance. To fix this, if it is fixable by the ion optics, one would need to redesign the meniscus-forming electrode shapes to better suit the conditions. Unfortunately designing the optics taking these effects in account would require the use of tools capable of correctly reproducing the conditions at the plasma sheath, i.e. the PIC Monte Carlo codes.

## 5. Summary and conclusion

Three extraction systems for the Linac4 $H^-$ion source were discussed. Each iteration aimed at improving the electron dumping efficiency and the beam properties for increased transmission through the RFQ over the previous version.

It was observed that the dumping efficiency of IS02 was not sufficient. An intense electron current was observed at the einzel lens downstream of the electron dump. Modifying the magnetic field with a magnetic shield at the plasma electrode and additional dipole magnets in the dump improved the dumping efficiency of IS03a significantly. However, in this case, the measured $e/H^-$ ratio was significantly higher than for IS02, which is explained by the reduced filter field strength inside the plasma chamber. To overcome these conflicting effects, the *puller-dump* of IS03b was completely redesigned: the magnetic shield was moved to the *puller-dump* to not compromise the filter field close to the plasma electrode and the size of the electron dump was increased. With these modifications, the dumping efficiency was improved to up to 100% in the case of IS03b as predicted by simulations and as observed during operation where no secondary-electron induced current was measured on the einzel lens.

The geometries of the *puller-dump* and einzel lens were optimized for a reduced beam and emittance growth: for IS03a and IS03b the extraction system was shortened and the accelerating einzel lens was optimized for a reduced beam size and divergence at the entrance of the LEBT. For the nominal IS03b settings, the simulated transport efficiency is about 88% and is satisfying the design criteria of 40 mA inside the RFQ acceptance.

The measured transport efficiency through the RFQ will likely be lower because of the slightly stronger effective magnetic field strength of the *puller-dump*, reduced voltage of the einzel lens and the simplified hypothesis of IBSimu not accounting for $H^-$ surface emission. These effects lead to aberration, population of the beam halo, increased emittance and losses at the LEBT walls.

Therefore, it is necessary to further enhance the performance of the $H^-$ injection into the RFQ. The source, the extraction system, and the LEBT must be treated as an entity to study and optimize their combined and interrelated effects. The beam extraction from the plasma needs to be optimized accounting for surface emission and non-linear forces. The focusing strength of the einzel lens could be improved by optimizing the plasma electrode and the *puller-dump* to a larger beam size and by increasing the einzel lens potential if the limitations set by sparking can be overcome.

The most straight-forward means to improve the transmission through the LEBT and matching to the RFQ acceptance is to correct for the beam angle that is induced by the magnetic field of the *puller-dump*. Simulations predict that offsetting this effect by tilting the source and the *puller-dump* with respect to the beam axis could lead to significantly improved transport efficiencies through the RFQ.

In view of the high plasma density and specific boundary conditions, a particle-in-cell simulation of the plasma coupled to the extraction system would provide a more accurate albeit more challenging description.

In conclusion, a novel and very effective *puller-dump* for $H^-$ sources was successfully designed, tested and operated at Linac4. Simulations of the beam trajectories are in decent agreement with the measurements, verifying IBSimu as a design tool for high-intensity negative ion-beam extraction and transport systems.

The design request of safely dumping the co-extracted electrons is satisfied with the new magnetic configuration and the dump geometry.

## Acknowledgments

We acknowledge the support of the Linac4 scientific and technical teams for providing excellent support in the development and operation of the Linac4 $H^-$ source and extraction systems. T. Kalvas acknowledges the support from the Academy of Finland under the Finnish Center of Excellence Program 2012–2017 (Nuclear and Accelerator Based Physics Research at JYFL).

## References

[1] L. Arnaudon, P. Baudrenghien, C. Bertone, Y. Body, J. Broere, O. Brunner, M. Buzio, C. Carli, F. Caspers, J. Corso, J. Coupard, A. Dallocchio, N. Dos Santos, R. Garoby, F. Gerigk, L. Hammouti, K. Hanke, M. Jones, I. Kozsar, J. Lettry, J. Lallement, A. Lombardi, L. Lopez-Hernandez, C. Maglioni, S. Mathot, S. Maury, B. Mikulec, D. Nisbet, C. Noels, M. Paoluzzi, B. Puccio, U. Raich, S. Ramberger, C. Rossi, N. Schwerg, R. Scrivens, G. Vandoni, S. Weisz, J. Vollaire, M. Vretenar, T. and Zickler, Proc. IPAC2011 CERN-ATS-2011-041, 2011, 4 p. URL: https://cds.cern.ch/record/1378473.

[2] L. Arnaudon, P. Baudrenghien, M. Baylac, G. Bellodi, Y. Body, J. Borburgh, P. Bourquin, J. Broere, O. Brunner, L. Bruno, C. Carli, F. Caspers, S.M. Cousineau, Y. Cuvet, C. De Almeida Martins, T. Dobers, T. Fowler, R. Garoby, F. Gerigk, B. Goddard, K. Hanke, M. Hori, M. Jones, K. Kahle, W. Kalbreier, T. Kroyer, D. Küchler, A.M. Lombardi, L.A. Lopez-Hernandez, M. Magistris, M. Martini, S. Maury, E. Page, M. Paoluzzi, M. Pasini, U. Raich, C. Rossi, J.P. Royer, E. Sargsyan, J. Serrano, R. Scrivens, M. Silari, M. Timmins, W. Venturini-Delsolaro, M. Vretenar, R. Wegner, W. Weterings, T. Zickler, Linac4 Technical Design Report, Technical Report CERN-AB-2006-084. CARE-Note-2006-022-HIPPI, CERN, Geneva, 2006, URL: https://cds.cern.ch/record/1004186, revised version submitted on 2006-12-14 09:00:40.

[3] M. Bacal, A. Hatayama, J. Peters, IEEE Trans. Plasma Sci. 33 (2005) 1845–1871. http://dx.doi.org/10.1109/TPS.2005.860069.

[4] Y.I. Belchenko, G.I. Dimov, V.G. Dudnikov, A.A. Ivanov, Dokl. Akad. Nauk SSSR 213 (1973) 1283.

[5] M. Bacal, M. Wada, Appl. Phys. Rev. 2 (2015) 021305. http://dx.doi.org/10.1063/1.4921298.

[6] J. Lettry, D. Aguglia, Y. Coutron, E. Chaudet, A. Dallocchio, J.G. Flores, J. Hansen, E. Mahner, S. Mathot, S. Mattei, Ø. Midttun, P. Moyret, D. Nisbet, M. O'Neil, M. Paoluzzi, C. Pasquino, H. Pereira, J.S. Arias, C. Schmitzer, R. Scrivens, D. Steyaert, AIP Conf. Proc. 1515 (2013) 302–311. http://dx.doi.org/10.1063/1.4792798.

[7] H. Damerau, A. Funken, R. Garoby, S. Gilardoni, B. Goddard, K. Hanke, A. Lombardi, D. Manglunki, M. Meddahi, B. Mikulec, G. Rumolo, E. Shaposhnikova, M. Vretenar, J. Coupard, LHCInjectors Upgrade, Technical.Design Report, Vol. I: Protons, Technical Report CERN-ACC-2014-0337, CERN, 2014, URL: http://cds.cern.ch/record/1976692.

[8] J. Lettry, D. Aguglia, J. Alessi, P. Andersson, S. Bertolo, A. Butterworth, Y. Coutron, A. Dallocchio, N. David, E. Chaudet, D.A. Fink, J. Gil-Flores, M. Garlasche, A. Grudiev, R. Guida, J. Hansen, M. Haase, A. Hatayama, A. Jones, I. Koszar, T. Lehn, C. Machado, C. Mastrostefano, S. Mathot, S. Mattei, Ø. Midttun, P. Moyret, D. Nisbet, K. Nishida, M. O'Neil, M. Paoluzzi, J.S. Alvarez, R. Scrivens, T. Shibata, D. Steyaert, N. Thaus, A. Zelenski, AIP Conf. Proc. 1655 (2015) 030005. http://dx.doi.org/10.1063/1.4916432.

[9] K.N. Leung, M. Bacal, Rev. Sci. Instrum. 55 (1984) 338–341. http://dx.doi.org/10.1063/1.1137762.

[10] Ø. Midttun, T. Kalvas, M. Kronberger, J. Lettry, H. Pereira, R. Scrivens, AIP Conf. Proc. 1515 (2013) 481–490. http://dx.doi.org/10.1063/1.4792819.

[11] S. Mochalskyy, J. Lettry, T. Minea, New J. Phys. 18 (2016) 085011. http://dx.doi.org/10.1088/1367-2630/18/8/085011.

[12] S. Nishioka, S. Abe, S. Mattei, J.B. Lallement, T. Kalvas, A. Hatayama, J. Lettry, AIP Conf. Proc. (2018) Proceedings of the International Conference of Ion Sources 2017, in press.

[13] T. Kalvas, O. Tarvainen, T. Ropponen, O. Steczkiewicz, J. Ärje, H. Clark, Rev. Sci. Instrum. 81 (2010) 02B703. http://dx.doi.org/10.1063/1.3258608.

[14] T. Kalvas, Development and Use of Computational Tools for Modelling Negative Hydrogen Ion Source Extraction Systems (Ph.D. thesis), Dept. of Physics, University of Jyväskylä, 2013, URL: www.jyu.fi/static/fysiikka/vaitoskirjat/2013/Kalvas-Taneli-pdf.

[15] C.A. Valerio-Lizarraga, I. Leon-Monzon, R. Scrivens, Phys. Rev. ST Accel. Beams 18 (2015) 080101. http://dx.doi.org/10.1103/PhysRevSTAB.18.080101.

[16] Cobham plc., Vector fields opera, 2014, URL: http://www.cobham.com/.

[17] M. Kronberger, E. Chaudet, G. Favre, J. Lettry, D. Küchler, P. Moyret, M. Paoluzzi, L. Prever-Loiri, C. Schmitzer, R. Scrivens, D. Steyaert, AIP Conf. Proc. 1390 (2011) 255–264. http://dx.doi.org/10.1063/1.3637395.

[18] J. Lettry, J. Alessi, D. Faircloth, A. Gerardin, T. Kalvas, H. Pereira, S. Sgobba, Rev. Sci. Instrum. 83 (2012) 02A728. http://dx.doi.org/10.1063/1.3680078.

[19] S. Briefi, D.A. Fink, S. Mattei, J. Lettry, U. Fantz, Rev. Sci. Instrum. 87 (2016) 02B104. http://dx.doi.org/10.1063/1.4932009.

[20] S. Briefi, S. Mattei, D. Rauner, J. Lettry, M.Q. Tran, U. Fantz, New J. Phys. 19 (2017) 105006. http://dx.doi.org/10.1088/1367-2630/aa8679.

[21] R. Scrivens, G. Bellodi, O. Crettiez, V. Dimov, D. Gerard, E.G. Souza, R. Guida, J. Hansen, J.-B. Lallement, J. Lettry, A. Lombardi, Ø. Midttun, C. Pasquino, U. Raich, B. Riffaud, F. Roncarolo, C.A. Valerio-Lizarraga, J. Wallner, M.Y. Satri, T. Zickler, Rev. Sci. Instrum. 85 (2014) 02A729. http://dx.doi.org/10.1063/1.4847195.

[22] B. Cheymol, E. Bravin, C. Dutriat, A. Lokhovitsky, U. Raich, F. Roncarolo, R. Scrivens, E. Zorin, Proceedings of the 1st International Particle Accelerator Conference, 2010, 3 p, URL: https://cds.cern.ch/record/1271728.

[23] D.A. Fink, J. Lettry, Ø. Midttun, R. Scrivens, D. Steyaert, C.A. Valerio-Lizarraga, AIP Conf. Proc. 1655 (2015) 030006. http://dx.doi.org/10.1063/1.4916433.